Characterization of Neoplastic Cells in the Cystic Space of Invasive Micropapillary Carcinoma of the Canine Mammary Gland.

Michele Angela Rodrigues
Universidade Federal de Minas Gerais
Andre L. Caldeira-Brant
Universidade Federal de Minas Gerais
Dawidson Assis Gomes
Universidade Federal de Minas Gerais
Tatiany L. Silveira
Universidade Federal de Minas Gerais
Hélio Chiarini-Garcia
Universidade Federal de Minas Gerais
Geovanni Dantas Cassali (cassalig@icb.ufmg.br)
Universidade Federal de Minas Gerais https://orcid.org/0000-0002-5650-6743

Research article

Keywords: Invasive micropapillary carcinoma, super-resolution microscopy, transmission electron microscopy, canine mammary gland, cancer, tumor microenvironment

Posted Date: July 23rd, 2020

DOI: https://doi.org/10.21203/rs.3.rs-46843/v1

Version of Record: A version of this preprint was published on March 24th, 2021. See the published version at https://doi.org/10.1186/s12917-021-02807-y.

Abstract

Background: Invasive micropapillary carcinoma (IMPC) is a rare breast malignant tumor and a variant form of invasive ductal carcinoma that is an aggressive neoplasm of the canine mammary gland and the human breast. There is a progressed recognition of the importance of the tumor microenvironment in cancer development, but little is known about cell types expressed in the cystic space of canine IMPC. This study aimed to investigate the neoplastic and stromal cells surrounding the cystic space in IMPC.

Methods: It was used immunohistochemistry (IHC), immunofluorescence (IF), super-resolution microscope and transmission electron microscopy (TEM) to access the localization and morphology of both stromal cells and epithelial cells in canine IMPC cystic areas.

Results: Cells surrounding the cystic space in IMPC were positive for the mesenchymal marker's alpha-smooth muscle actin (aSMA), Vimentin, and S100A4. Furthermore, myoepithelial cell marker p63 was negative on IMPC. Tumoral reversal polarity was observed using MUC1 for the first time in IMPC from the canine mammary gland. MUC1 is known to have a role in lumen formation and has an inhibitory role in the cell to stroma interaction. TEM showed that cells lining the IMPC cystic space were modified myoepithelial cells.

Conclusion: The present work demonstrates, for the first time, a characterization of the cystic space compound on IMPC from the canine mammary gland. These findings could be useful to understand better the cellular microenvironment in invasive tumors of the mammary gland to improve cancer treatment.

Background

One of the most aggressive types of breast cancer is invasive micropapillary carcinoma (IMPC). That is a morphologically distinctive and rarely observed form of invasive ductal carcinoma composed of small and moruliform-like clusters of cancer cells, surrounded by clear stromal spaces that presents lymphotropism and aggressive behavior [1, 2]. Previous work, evaluating canine IMPC showed several similarities to the human counterpart, for example, high histological grade, a high incidence of lymph node metastasis and low overall survival rates were observed [3–6]. These and other observations demonstrated that the canine mammary gland might be an adequate model for human breast cancer comparative pathology [7].

Emerging evidence is showing differences in the tumor microenvironment that contribute to the mechanisms to generate suppressive or tolerant environments that allow tumor regression or progression. The tumor microenvironment is composed of the tumor cells and non-tumor surrounding cells, blood vessels, extracellular matrix and a variety of biologically active molecules derived from tumor and non-tumor cells [8]. The heterogeneity, dynamic localization, and differentiation process of the mammary gland cells surrounding the cystic space in IMPC, as well as the transformation of

carcinomatous areas *in situ* to invasive, still poorly understood for the development and treatment of breast cancer.

In the normal breast, the ductal epithelium and the underlying myoepithelial cells are separated by a basement membrane from the surrounding connective tissue that contains capillaries, fibrillar extracellular matrix and fibroblasts. During invasive ductal carcinomas, the basement membrane is ruptured, and the tumor cells often form irregular duct-like areas without a defined basement membrane. The stroma surrounding the tumor cells contains inflammatory infiltrate, newly formed capillaries and myofibroblasts [9].

The stromal cells have been shown to have a deep effect on normal and tumoral tissue and may play a key role in regulating breast epithelial cell function [10]. Resting and activated fibroblasts are associated with cancer cells at all stages of cancer progression, their structural and functional contributions to this process are beginning to emerge — so-called cancer-associated fibroblasts (CAFs) [11, 12]. Many molecules are used as CAF markers such as α-smooth muscle actin (αSMA), an important marker for differentiated myofibroblasts [8, 13, 14]; S100A4, also named as fibroblast specific protein-1 (FSP-1), is a calcium-binding protein and has been recognized as a key player in tumor progression and metastasis [15]; and Vimentin an intermediate-filament associated protein [9].

Invasive micropapillary carcinoma demonstrates an unexpected secretory activity in the stroma-facing surface of the tumor cells suggesting a reversal in cell polarity in this type of tumor [1]. Nassar et al. (2004) presented a study showing the distribution of MUC1, which is a type of mucin (a surface glycoprotein) in human IMPC from different organs. This study characterized a reversal of cellular polarization and expression of MUC1 in the stroma-facing surface of the cells [2]. The cell polarity alteration demonstrated by electron microscopy of breast carcinomas showing the presence of many microvilli at the surface of the cells facing the stroma [1].

In this work, we investigate the expression markers of neoplastic and stromal cells surrounding the cystic space in canine IMPC using IHC, immunofluorescence, confocal and super-resolution microscopy and TEM. Together these results suggest the importance of cells with mesenchymal background for IMPC development and to understand the cystic space microenvironment for improvement of IMPC treatment.

Methods

Case Selection, Histopathological Analysis, and Overall Survival

Four cases of IMPC and one control of canine mammary gland were selected at the Laboratory of Comparative Pathology of the Institute of Biological Sciences, "Universidade Federal de Minas Gerais" (UFMG), after approval by Animal Experimentation Ethics Committee (CEUA protocol number:362/2016).

For histopathological analysis (grading), primary tumor specimens were fixed in 10% neutral buffered formalin, paraffin-embedded (FFPE), and 4 µm thick histological sections were cut and stained with

hematoxylin and eosin. All cases were reviewed and re-classified independently by two pathologists (GDC and TS). In brief, carcinomas with cystic formations containing nests of epithelial cells with a moruliform appearance (infiltrating micropapillary pattern) were diagnosed as IMPC, associated or not with *in situ* micropapillary areas [16] (**Figure 1**). The invasive areas of canine IMPC were graded according to the Nottingham grading system [17, 18]. The overall survival time ranged from 8 to 150 days (median 71 days).

Immunohistochemistry

Immunohistochemistry was performed as previously described with minor modifications [7, 19]. Sections (4 µm) of primary tumors were mounted on silanized slides, and a peroxidase-based detection system, Novolink™ Polymer, was applied (Novolink™ Polymer Detection System, Leica Biosystems Newcastle Ltd., Newcastle, UK). The slides were dewaxed in xylene, and endogenous peroxidase activity was blocked with 3% H_2O_2 in methanol. The reagents were applied manually, and immunoreactivity was visualized by incubating the slides with 3,3'-diaminobenzidine (Lab Vision DAB substrate system; Lab Vision, Fremont, California, USA) for 5 min. The antibodies used were mouse monoclonal anti-cytokeratin (clone 34bE12, Dako, 1:100) and anti CD31, p63, and anti-vimentin, as described above. Negative controls were performed using a normal serum (Lab Vision Ultra V Block) in place of the primary antibody. For all markers, the immunohistochemical analysis was performed on *in situ* and invasive areas.

Phenotypic markers immunofluorescence and imaging by super-resolution microscopy

Immunofluorescence was performed for aSMA, Vimentin, CD31, Von Willebrand Factor, p63, S100A4, Lamin B1 or B2, and MUC1, as previously described in Rodrigues M.A. et al. (2016) [20–23]. Brief, FFPE tissue sections were dewaxed, rehydrated, and unmasked in trilogy solution (Cell Marque, Koclin, CA, USA) in pressurized heating (125ºC) for 20 minutes according to manufacturer's instructions. Next, samples were rinsed in Phosphate Buffered Saline (PBS, 137 mM NaCl, 2.7 mM KCl and 10 mM phosphate buffer solution, pH 7.4) (Sigma-Aldrich, Carlsbad, CA, USA) and incubated in PBS containing 0.2% Triton X-100 (Sigma-Aldrich) for another 20 minutes, then blocked in PBS containing 1% Bovine Serum Albumin (BSA, Sigma-Aldrich) for 30 minutes. Next, The sections were incubated with a rabbit polyclonal antibody against the nuclear envelope marker Lamin B1 (1:1000, Abcam, Cambridge, MA, USA) or with a mouse monoclonal antibody against Lamin B2 (1:100, Life Technologies) overnight at 4ºC, and with one of the following antibodies: a mouse monoclonal antibody against aSMA (1:100, clone 1A4, Dako, Denmark); a mouse monoclonal antibody against Vimentin (1:100, clone Vim 3B4, Dako, Denmark); a mouse monoclonal antibody against CD31 (1:100, clone JC70A, Dako, Denmark); a rabbit polyclonal antibody against Von Willebrand Factor (1:800, Dako, Denmark); a mouse monoclonal antibody against p63 (1:100, clone 4A4, NeoMarkers, CA, USA); a rabbit polyclonal antibody against S100A4 (1:100, Life Technologies, Carlsbad, CA, USA); and or with a rabbit polyclonal antibody against MUC1 (clone EP1024Y) (1:100, Abcam, USA). They were then rinsed three times for 5 minutes in PBS. Subsequently, sections were incubated with Alexa Fluor® 488 Goat Anti-Rabbit IgG antibody (1:1000, Life Technologies), Alexa Fluor® 555 Goat anti-mouse IgG antibody (1:1000, Life Technologies) and Hoechst

33258 (1 mg/mL, Life Technologies) for 1 hour at room temperature. Next, samples were washed 3x in PBS for 10 minutes and then mounted in Prolong Gold Antifade reagent (Life Technologies). The negative control was included in all reactions by omitting primary antibodies. Images were collected using a Zeiss LSM 880 with Airyscan (Carl Zeiss, Jena, Germany) using an oil 40x 1.3 NA objective lens. Samples were excited at 405 nm and observed at 420-480 nm to detect Hoechst, at 488 nm and observed at 500-525 nm to detect Alexa Fluor 488, at 543 nm and observed using LP 570 nm to detect Alexa Fluor 555 signal. The software Zeiss Efficient Navigation (ZEN) was used for orthogonal projections (XY, XZ, YZ). The fluorescence microscopy results were evaluated in 10 invasive areas of IMPC and were collected ten images from each case (n = 100).

Tissue processing for ultrastructural evaluation

For transmission electron microscopy (TEM), one health and tumor biopsies (it was selected five fields of each) fixed by 10% neutral buffered formalin were cut into approximately 2 mm (length x width) and subsequently post-fixed in 5% glutaraldehyde (biological grade; Electron Microscopy Sciences, Hatfield, PA, USA) in 0.05M phosphate buffer pH 7.3 for 24 h. After that, the fragments were post-fixed in reduced osmium (osmium tetroxide 1% and potassium ferrocyanide in distilled water) for 90 min, dehydrated in ethanol and acetone before embedding in epoxy Araldite resin (Electron Microscopy Sciences, Hatfield, PA, USA). From ultrathin sections of 60 nm of thickness were obtained images using a Tecnai G-12 FEI – 120 Kv microscope. The images were adjusted for resolution, sharpness, and contrast using Adobe Photoshop (Adobe System, Inc, Mountain View, CA, USA).

Results

Anatomopathological description

IMPC cases were selected from the Laboratory of Comparative Pathology archives **(Figure 1)**. The age of animals ranged from 4 to 13 years (mean 10.5 ± 3) at the time of surgery. Tumors smaller than 5 cm were predominant (2/4, 50%), and regional metastasis was observed in 75% of the dogs (3/4). Regarding the IMPC histopathological analysis, all cases showed histological grade II. Concerning overall survival, three dogs died because of mammary neoplasia, and one dog died due to a hemorrhagic diathesis. The overall survival time ranged from 8 to 150 days (median 71 days). The clinicopathological and survival findings of the canines are presented in **Table 1**. One health canine mammary gland sample was used as a control.

Immunohistochemical analysis

Immunohistochemical analyses were performed in all primary IMPCs, and images were observed by light microscopy. All IMPC cases demonstrated numerous irregular stromal cystic formations containing nests of epithelial cells in a morula pattern **(Figure1)**. The lumen presented cell clusters on the *in situ* areas, the transition to invasive areas and the neoplastic cells were pleomorphic with typically polygonal morphology. We observed CK staining, showing the epithelial compound on IMPC **(Figure 2, A**

and B). We used vimentin staining to investigate the cellular localization of the stromal compound surrounding the IMPC, and this marker was observed at the plasma membrane of the mesenchymal cells around the IMPC areas **(Figure 2C)**. The p63 staining for myoepithelial cells was negative on IMPC **(Figure 2D),** and this suggests the presence of only epithelial cells on IMPC nests. CD31 staining was positive in the pre-existing vascular spaces around the tumor, and not observed in IMPC cystic formations **(Figure 2, E and F)**. Together these results demonstrate the presence of epithelial cells (CK^{+}) on IMPC cystic space, the mesenchymal compound ($vimentin^{+}$), and the absence of myoepithelial ($p63^{-}$) and endothelial ($CD31^{-}$) cells on IMPC.

Phenotypical characterization of stromal and neoplastic cells by super-resolution microscopy

To overcome the image resolution limitations by conventional light microscopes and confocal systems, in 2014, the 2D detector array imaging system (DAIS) was improved by Zeiss in the LSM 880 system with the Airyscan detector. The super-resolution system also utilizes the linear deconvolution by properly weighing the image of each detector element to realize the three-dimensional (3D) resolution enhancement and has been applied to biomedical research and clinical diagnosis [24]. The observation of IHC does not allow precise colocalization of signals, nor can multiple colors be visualized simultaneously, and this is another advantage to use the fluorescence system [25]. In this study, we used the Airyscan system to achieve higher signal and better resolution.

To observe the expression of the stromal and neoplastic cells surrounding the IMPC cystic space, we performed double-labeling of each marker: S100A4, smooth muscle actin (aSMA), and Vimentin with Lamin B1/B2 in all micropapillary cases from the canine mammary gland. The Lamin B1/B2 was used as a marker of the inner nuclear membrane (INM). IMPC cases demonstrated numerous irregular stromal cystic formations containing nests of epithelial cells in a morula pattern. Our results show that all four IMPC cases tested, the plasma membrane of many neoplastic cells was positive for S100A4, SMA, and Vimentin in invasive and *in situ* areas **(Figure 3, A, B and C)**. Von Willebrand factor and CD31 positive staining were observed in the plasma membrane of lymphatic and endothelial cells respectively in the pre-existing vascular spaces around the tumor, and not observed in IMPC cystic formations **(Figure 4, A and B)**. Von Willebrand staining was positive only in lymphatic vessels near to the IMPC cystic area (see **Figure 4A**). Serial super-resolution images show the localization of the stromal cells surrounding the epithelial nests **(Figure 3 and 4).** Furthermore, myoepithelial cell marker p63 staining was negative in IMPC and positive in health mammary glands used as a positive control (see **Figure 4, C and D**). To test the reverse polarity on IMPC, we performed MUC1 staining, and it was positive and diffusely present in the stroma-facing (basal) surface of the neoplastic cell clusters in all IMPC of the canine mammary gland **(Figure 5, A and B)**. Together these results demonstrate using super-resolution microscopy and immunofluorescence for the first time a characterization of the stromal compound of cells surrounding the IMPC cystic space in the canine mammary gland.

Ultrastructure of health and IMPC myoepithelial cell

The healthy myoepithelial cells showed thin elongated cytoplasm tapering bipolar processes. Their nuclei were ovoid or elongated, and the cytoplasm was filled with scarce organelles and large amounts of myofilaments. The myoepithelial cells were joined to the stroma by hemidesmosomes along the evident basement membrane **(Figure 6A)**. In IMPC, it was possible to verify that cells lining the cystic space were modified myoepithelial cells. They showed smaller and flatter nucleus and very thin and long cytoplasmic extensions with reduced myofilaments and the absence of both intercellular junctions and basement membrane **(Figure 6B)**. It was observed that in addition to having a flattened nucleus **(Figure 6C)**, neoplastic myoepithelial cells have long and thin cytoplasmic extensions covering the large lumen area of the invasive cystic space **(Figure 6, D and E)**. We also observed neoplastic myoepithelial cells *in situ* areas of the IMPC cystic space (data not shown).

Discussion

IMPC of the breast is a morphologically distinct form of invasive ductal carcinoma found in women [2]. The constituent tumor cells are typically arranged in small clusters with a central lumen and micropapillae lacking fibrovascular cores extending into clear spaces. IMPC of the breast is extremely aggressive tumors and, based on previous studies from our group, appear to exhibit similar behavior in dogs [1, 3, 4, 6]. In this study, we did a morphological analysis using histochemical, immunofluorescence combined with super-resolution imaging and ultrastructural examination by TEM to characterize the stromal cell compound surrounding the IMPC cystic space on the canine mammary gland.

The tumor microenvironment is composed of several cell types, including endothelial cells, fibroblasts, myofibroblasts, and others. The stroma around invasive breast tumors is described to differ from the normal breast, with alterations in stromal protein synthesis [10]. Compared to normal tissue, cancer-associated fibroblasts express higher levels of proteins, such as αSMA and S100A4 [8]. Several differences in the stroma of invasive breast cancer are attributed to activated fibroblasts, also termed myofibroblasts, reflecting their acquisition of aSMA expression [26, 27]. In our study, we also observed atypical fibroblasts. We found aSMA expression on IMPC cystic areas, and it may be a marker of the more aggressive behavior of this type of tumor. S100A4 has been reported to be overexpressed in an advanced stage of thyroid carcinoma and the breast, gastric, pancreatic, lung cancer, and prostate cancer patients [15, 28–30].

The S100A4 expression was positive in both invasive areas of tumor transition (*in situ* to invasive) in the present study, and it may play a role in more advanced disease with lymph node metastasis. We also observed the positive staining for the intermediate filament associated protein vimentin on canine IMPC. Typically, fibroblasts appear as fusiform cells with a prominent actin cytoskeleton and vimentin intermediate filaments. The role of fibroblasts in the origin and initiation of cancer invasion is poorly understood. Epithelial-to-mesenchymal transition is a source for converting epithelial cells into fibroblast-like cells in various tissues. Fibroblasts might also have a role in metastasis, and therapies against CAFs are being considered to control cancer [9].

In our study, all canine IMPC cases demonstrated numerous irregular stromal cystic formations containing nests of epithelial cells in a moruliform pattern. Positive staining for CD31 and Von Willebrand factor was observed in the plasma membrane of only endothelial and lymphatic cells of the pre-existing vascular spaces in the region around the tumor, and it was not observed in the IMPC cystic formations. The empty spaces surrounding the micropapillae of the carcinoma cell nests were not surrounded by endothelial, myoepithelial cells, thus confirming the infiltrative micropapillary nature of the tumor [4, 31].

According to Tavassoli (1999), the most important feature for distinguishing a papilloma from a papillary carcinoma is the presence of a relatively uniform myoepithelial cell layer in the proliferating intraluminal component of the lesion, and the absence of the basal myoepithelial layer in the papillary processes almost always indicates a carcinoma [32]. Several newer markers, including p63, have been used to identify the myoepithelial cell successfully. Identification of a myoepithelial cell layer histologically or by immunolocalization analysis has become a key feature in distinguishing benign from malignant and *in situ* from invasive lesions of the breast [33]. The p63 shows no cross-reactivity with myofibroblasts or vascular smooth muscle [33]. In our study, we observed negative staining for p63 in IMPC in all cases analyzed (see Fig. 4). Hill and Yeh (2005) showed that p63 was completely negative in invasive papillary carcinoma, and it was irregularly spaced nuclear staining with occasional gaps in intraductal papillomas [33]. Gamba et al. (2013) demonstrated a positive nuclear p63 staining in 20% of IMPC cases of the canine mammary gland by IHC [4]. We observed that careful background adjustments in the immunofluorescence, using the negative controls, decrease the chances of false-positive found in IHC samples. In our study under TEM, it was possible to identify cells lining the IMPC cystic space that were modified myoepithelial cells, and that could explain the negative p63 staining observed in the immunofluorescence, once we did not have access to a specific antibody for modified myoepithelial cells. The TEM, in our study, demonstrated that the neoplastic myoepithelial cells have long and thin cytoplasmic extensions covering the large lumen area of the invasive cystic space on canine IMPC.

IMPC cases can also show an unexpected secretory activity in the stroma-facing surface of the tumor cells suggesting a reversal in cell polarity. Other groups investigated the MUC1 distribution, and it was expressed in the apical surface of several types of epithelial tissues [2, 34]. We did a new observation showing MUC1 expression in the stroma-facing surface of the canine tumoral cells. It confirms the reversal of cellular polarization using immunofluorescence and super-resolution, and our findings were similar to what was observed in human IMPC. MUC1 expression in the stroma-facing surface of the cells could be one of the key factors in the distinctive morphology of this tumor type by causing the detachment of the neoplastic cells from the stroma [2].

Conclusions

The present work is showing a detailed morphological, immunocytochemical, and ultrastructural characterization analysis of stromal and neoplastic cells in IMPC. These cells can be attributed to rest or activated fibroblasts that can play an important role in this type of neoplasia. The micropapillary pattern in breast and canine mammary gland carcinoma is a distinct histopathological variant with prognostic

and biological significance. This entity should be more carefully recognized on pathological diagnosis for comparative studies.

Abbreviations

IMPC
Invasive micropapillary carcinoma, IHC:immunohistochemistry, IF:immunofluorescence, TEM:transmission electron microscopy, CAFs:cancer-associated fibroblasts, FFPE:paraffin-embedded, INM:inner nuclear membrane, αSMA:α-smooth muscle actin, S100A4:fibroblast specific protein-1 (FSP-1), MUC1:Mucin 1, CD31:cluster of differentiation 31, CK:Cytokeratin, p63:transformation-related protein 63, ZEN:Software Zeiss Efficient Navigation, DAIS:2D detector array imaging system, BSA:bovine serum albumin.

Declarations

Acknowledgments

The microscopic data shown in this work was obtained using the microscopes of *Centro de Aquisição e Processamento de Imagens* (CAPI - ICB/UFMG) and *Centro de Microscopia* (CM-UFMG).

Authors' contributions

MAR performed the fluorescence and super-resolution imaging experiments, participated in the coordination of the study, and wrote the final manuscript. ACB and HCG performed TEM experiments and analyses. DAG participated in the experiments and helped with the fluorescence imaging analyses. TS performed the IHC experiments. GDC, HCG, ACB, MAR, and DAG reviewed the entire manuscript. MAR and GDC conceived and designed the study. GDC and TS were responsible for histopathological examination. All authors read and approved the manuscript.

Funding

This work was supported by grants from CNPq, FAPEMIG, and CAPES. The funding sources had no role in writing, data collection, analysis, or interpretation, or any aspect pertinent to the study.

Availability of data and materials

Not applicable.

Ethics approval and consent to participate

The approval of the current study was granted by the Animal Experimentation Ethics Committee (CEUA) under the protocol number:362/2016, Universidade de Minas Gerais. It was a retrospective study, and all

samples used in this study were from the archive of the 'Laboratório de Patologia Comparada.' The Ethics Committee waived the need for consent.

Consent for publication

Not applicable.

Competing interests

The authors declare that they have no competing interests.

Author details

[1]Department of General Pathology, Universidade Federal de Minas Gerais, Av. Antônio Carlos 6627, Belo Horizonte, Minas Gerais, CEP: 31270-901, Brazil. [2]Department of Morphology, Universidade Federal de Minas Gerais, Av. Antônio Carlos 6627, Belo Horizonte, Minas Gerais, CEP: 31270-901, Brazil. [3]Department of Biochemistry and Immunology, Universidade Federal de Minas Gerais, Av. Antônio Carlos 6627, Belo Horizonte, Minas Gerais, CEP: 31270-901, Brazil.

References

1. Luna-Moré S, Gonzalez B, Acedo C, Rodrigo I, Luna C. Invasive micropapillary carcinoma of the breast. Pathol - Res Pract. 1994;190:668–74. doi:10.1016/S0344-0338(11)80745-4.
2. Nassar H, Pansare V, Zhang H, Che M, Sakr W, Ali-Fehmi R, et al. Pathogenesis of invasive micropapillary carcinoma: role of MUC1 glycoprotein. Mod Pathol. 2004;17:1045–50. doi:10.1038/modpathol.3800166.
3. Cassali GD, Serakides R, Gärtner F, Schmitt FC. Invasive micropapillary carcinoma of the dog mammary gland: a case report. Arq Bras Med Veterinária e Zootec. 2002;54:366–9. doi:10.1590/S0102-09352002000400006.
4. Gamba CO, Dias EJ, Ribeiro LGR, Campos LC, Estrela-Lima A, Ferreira E, et al. Histopathological and immunohistochemical assessment of invasive micropapillary mammary carcinoma in dogs: A retrospective study. Vet J. 2013;196:241–6. doi:10.1016/j.tvjl.2012.08.022.
5. Gamba CO, Campos LC, Negreiros-Lima GL, Maciel-Lima K, Sousa LP, Estrela-Lima A, et al. ZEB2 and ZEB1 expression in a spontaneous canine model of invasive micropapillary carcinoma of the mammary gland. Res Vet Sci. 2014;97:554–9. doi:10.1016/j.rvsc.2014.09.016.
6. Cassali GD, Gärtner F, Vieira da Silva MJ, Schmitt FC. Cytological diagnosis of a metastatic canine mammary tumor in pleural effusion. Arq Bras Med Veterinária e Zootec. 1999;51:307–10. doi:10.1590/S0102-09351999000400003.
7. de Oliveira Gamba C, Scaratti D, de Andrade VP, Estrela-Lima A, Ferreira E, Cassali GD. Invasive micropapillary carcinoma of the mammary gland in humans and canines: Clinicopathological,

immunophenotypical and survival approaches. Res Vet Sci. 2017;115 April:189–94. doi:10.1016/j.rvsc.2017.04.012.

8. Bussard KM, Mutkus L, Stumpf K, Gomez-Manzano C, Marini FC. Tumor-associated stromal cells as key contributors to the tumor microenvironment. Breast Cancer Res. 2016;18:84. doi:10.1186/s13058-016-0740-2.
9. Kalluri R, Zeisberg M. Fibroblasts in cancer. Nat Rev Cancer. 2006;6:392–401. doi:10.1038/nrc1877.
10. Chauhan H. There is more than one kind of myofibroblast: analysis of CD34 expression in benign, in situ, and invasive breast lesions. J Clin Pathol. 2003;56:271–6. doi:10.1136/jcp.56.4.271.
11. Franco OE, Shaw AK, Strand DW, Hayward SW. Cancer associated fibroblasts in cancer pathogenesis. Semin Cell Dev Biol. 2010;21:33–9. doi:10.1016/j.semcdb.2009.10.010.
12. Park CK, Jung WH, Koo JS. Expression of cancer-associated fibroblast-related proteins differs between invasive lobular carcinoma and invasive ductal carcinoma. Breast Cancer Res Treat. 2016;159:55–69. doi:10.1007/s10549-016-3929-2.
13. Desmouliere A, Guyot C, Gabbiani G. The stroma reaction myofibroblast: a key player in the control of tumor cell behavior. Int J Dev Biol. 2004;48:509–17. doi:10.1387/ijdb.041802ad.
14. De Wever O, Demetter P, Mareel M, Bracke M. Stromal myofibroblasts are drivers of invasive cancer growth. Int J Cancer. 2008;123:2229–38. doi:10.1002/ijc.23925.
15. Mishra SK, Siddique HR, Saleem M. S100A4 calcium-binding protein is key player in tumor progression and metastasis: preclinical and clinical evidence. Cancer Metastasis Rev. 2012;31:163–72. doi:10.1007/s10555-011-9338-4.
16. Cassali GD, Lavalle GE, Nardi a. De B, Ferreira E, Bertagnolli a C, Estrela-Lima A, et al. Consensus for the diagnosis, prognosis and treatment of canine mammary tumors. Brazilian J Vet Pathol. 2014;4:153–80.
17. Elston CW. EIO. Pathological prognostic factors in breast cancer. I. The value of histological grade in breast cancer: experience from a large study with long-term follow-up. Histopathology. 1991;19:403–10.
18. Elston CW EIO. Assessment of histological grade. In: Systemic Pathology—The Breast. Third. Elsevier Science Health Science Division; 1998. p. 365–384.
19. Gamba C, de O, Damasceno KA, Ferreira IC, Rodrigues MA, Gomes DA, Alves MR, et al. The investigation of transcriptional repression mediated by ZEB2 in canine invasive micropapillary carcinoma in mammary gland. PLoS One. 2019;14:e0209497. doi:10.1371/journal.pone.0209497.
20. Gamba CO, Rodrigues MA, Gomes DA, Estrela-Lima A, Ferreira E, Cassali GD. The Relationship Between E-Cadherin and its Transcriptional Repressors in Spontaneously Arising Canine Invasive Micropapillary Mammary Carcinoma. J Comp Pathol. 2015;153:256–65. doi:10.1016/j.jcpa.2015.08.006.
21. Faria JAQA, de Andrade C, Goes AM, Rodrigues MA, Gomes DA. Effects of different ligands on epidermal growth factor receptor (EGFR) nuclear translocation. Biochem Biophys Res Commun. 2016;478:39–45. doi:10.1016/j.bbrc.2016.07.097.

22. Rodrigues MA, Gamba CO, Faria JAQA, Ferreira Ê, Goes AM, Gomes DA, et al. Inner nuclear membrane localization of epidermal growth factor receptor (EGFR) in spontaneous canine model of invasive micropapillary carcinoma of the mammary gland. Pathol - Res Pract. 2016;212:340–4. doi:10.1016/j.prp.2015.11.017.
23. de Miranda MC, Rodrigues MA, de Angelis Campos AC, Faria JAQA, Kunrath-Lima M, Mignery GA, et al. Epidermal growth factor (EGF) triggers nuclear calcium signaling through the intranuclear phospholipase Cδ-4 (PLCδ4). J Biol Chem. 2019;294:16650–62. doi:10.1074/jbc.RA118.006961.
24. LI Y, LIU S, LIU D, SUN S, KUANG C, DING Z, et al. Image scanning fluorescence emission difference microscopy based on a detector array. J Microsc. 2017;266:288–97. doi:10.1111/jmi.12538.
25. 10.1101/pdb.prot5503
Bashaw GJ. Visualizing Axons in the Drosophila Central Nervous System Using Immunohistochemistry and Immunofluorescence. Cold Spring Harb Protoc. 2010;2010:pdb.prot5503-pdb.prot5503. doi:10.1101/pdb.prot5503.
26. Grinnell F. Fibroblasts, myofibroblasts, and wound contraction. J Cell Biol. 1994;124:401–4. doi:10.1083/jcb.124.4.401.
27. Kuroda N, Sugimoto T, Takahashi T, Moriki T, Toi M, Miyazaki E, et al. Invasive Micropapillary Carcinoma of the Breast: An Immunohistochemical Study of Neoplastic and Stromal Cells. Int J Surg Pathol. 2005;13:51–5. doi:10.1177/106689690501300107.
28. Gupta S, Hussain T, MacLennan GT, Fu P, Patel J, Mukhtar H. Differential Expression of S100A2 and S100A4 During Progression of Human Prostate Adenocarcinoma. J Clin Oncol. 2003;21:106–12. doi:10.1200/JCO.2003.03.024.
29. Zou M, Al-Baradie RS, Al-Hindi H, Farid NR, Shi Y. S100A4 (Mts1) gene overexpression is associated with invasion and metastasis of papillary thyroid carcinoma. Br J Cancer. 2005;93:1277–84. doi:10.1038/sj.bjc.6602856.
30. Ismail NI, Kaur G, Hashim H, Hassan MS. S100A4 overexpression proves to be independent marker for breast cancer progression. Cancer Cell Int. 2008;8:12. doi:10.1186/1475-2867-8-12.
31. Pettinato G, Manivel CJ, Panico L, Sparano L, Petrella G. Invasive Micropapillary Carcinoma of the Breast: Clinicopathologic Study of 62 Cases of a Poorly Recognized Variant With Highly Aggressive Behavior. Am J Clin Pathol. 2004;121:857–66. doi:10.1309/XTJ7-VHB4-9UD7-8X60.
32. Tavassoli F. Papillary lesions. Pathology of the Breast. 2nd ed. New York: McGraw-Hill. 1999. pp. 325–71.
33. Hill CB, Yeh I-T. Myoepithelial Cell Staining Patterns of Papillary Breast Lesions. Am J Clin Pathol. 2005;123:36–44. doi:10.1309/XG7TPQ16DMJAV8P1.
34. Winterford CM, Walsh MD, Leggett BA, Jass JR. Ultrastructural Localization of Epithelial Mucin Core Proteins in Colorectal Tissues. J Histochem Cytochem. 1999;47:1063–74. doi:10.1177/002215549904700811.

Tables

Table 1. Clinicopathological and survival findings of the IMPCs of the canine mammary gland.

	Age (years)	Breed	Tumor Size (cm)	Lymph node Metastasis	Histological Grade*	Overall survival (days)#
Case 1 (37/12)	14	Poodle	5	Yes	II	71
Case 2 (19/12)	8	Daschound	4	Yes	II	150
Case 3 (1140/10)	12	Crossbreed	7	Yes	II	30
Case 4 (58/09)	8	Akita	4	NA	II	8§

NA, Not Available.

* Histological grading based on that of Elston and Ellis (Elston et al. 1991; Elston C. W. 1998).

The overall survival time was defined as the period (in days) between surgery and death due to the tumor. Three canines evaluated, died due to the disease; nevertheless, in case 4 (§), the bitch died because of a hemorrhagic diathesis.

Figures

Figure 1

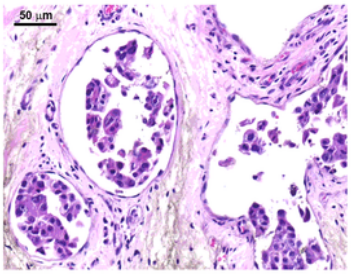

Figure 1

Histopathological appearance of the spontaneous canine model of invasive micropapillary carcinoma. Invasive and in situ micropapillary areas characterized by neoplastic epithelial cells within cystic spaces. Harris's hematoxylin stains (Scale bar = 50 m).

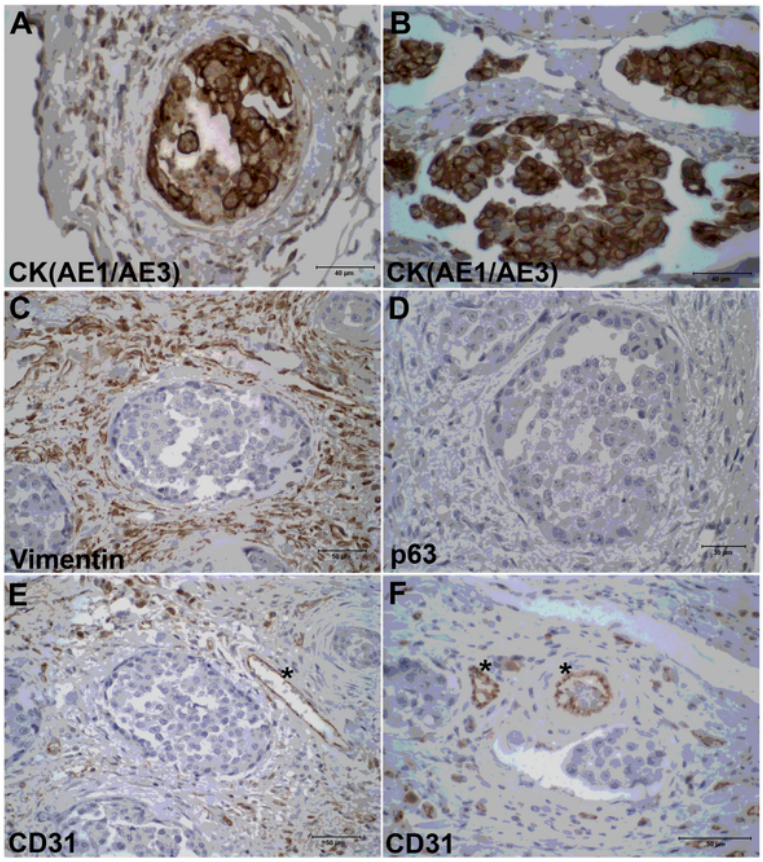

Figure 2

Figure 2

Photomicrographs illustrating Cytokeratin (AE1/AE3), Vimentin, p63, and CD31 immunostaining on IMPC the canine mammary gland. Epithelial neoplastic cells exhibiting Cytokeratin (AE1/AE3) positive staining on in situ and invasive areas of IMPC (see arrows) (A-B) (Scale bar = 40 □m). Vimentin positive labeling confirming the presence of a mesenchymal compound on IMPC (C) (Scale bar = 50 □m). Negative p63 staining on IMPC (D) (Scale bar = 30 □m). CD31 positive staining only in the plasma membrane of

endothelial cells (see asterisks) (E-F) (Scale bar = 50 μm). (Novolink™ Polymer Detection System, counterstained with Harris's hematoxylin).

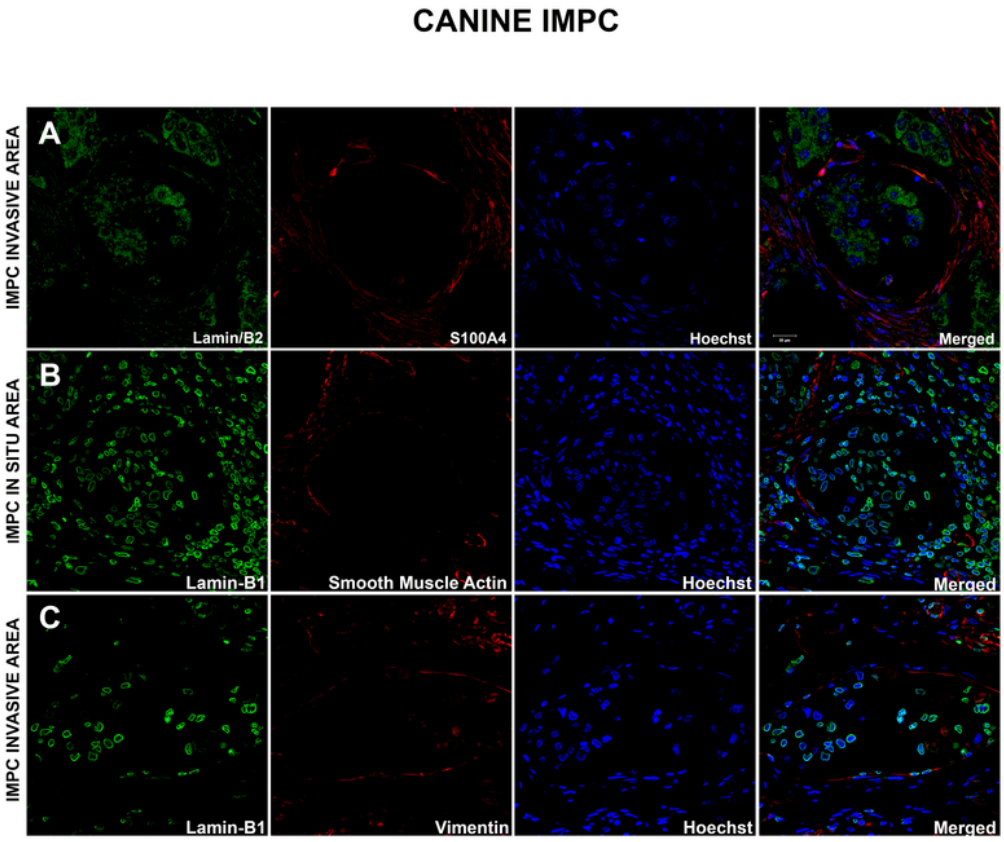

Figure 3

Figure 3

S100A4, αSMA, and vimentin expression in a spontaneous canine model of invasive areas of IMPC. Super-resolution images of the nuclear envelope marker Lamin B1/B2 (green), S100A4, α smooth muscle actin (αSMA), Vimentin (red) and the nucleus was stained with Hoechst (blue) in invasive (A-C) and in situ

areas (B). Note that the intermediate microfilaments staining is surrounding the cystic space of micropapillary tumoral areas. The merged images show the channels overlap. Images are representative of what was observed in n=40 separate primary tumor cases and were collected ten images from invasive areas of each case. Scale bars = 20 □m.

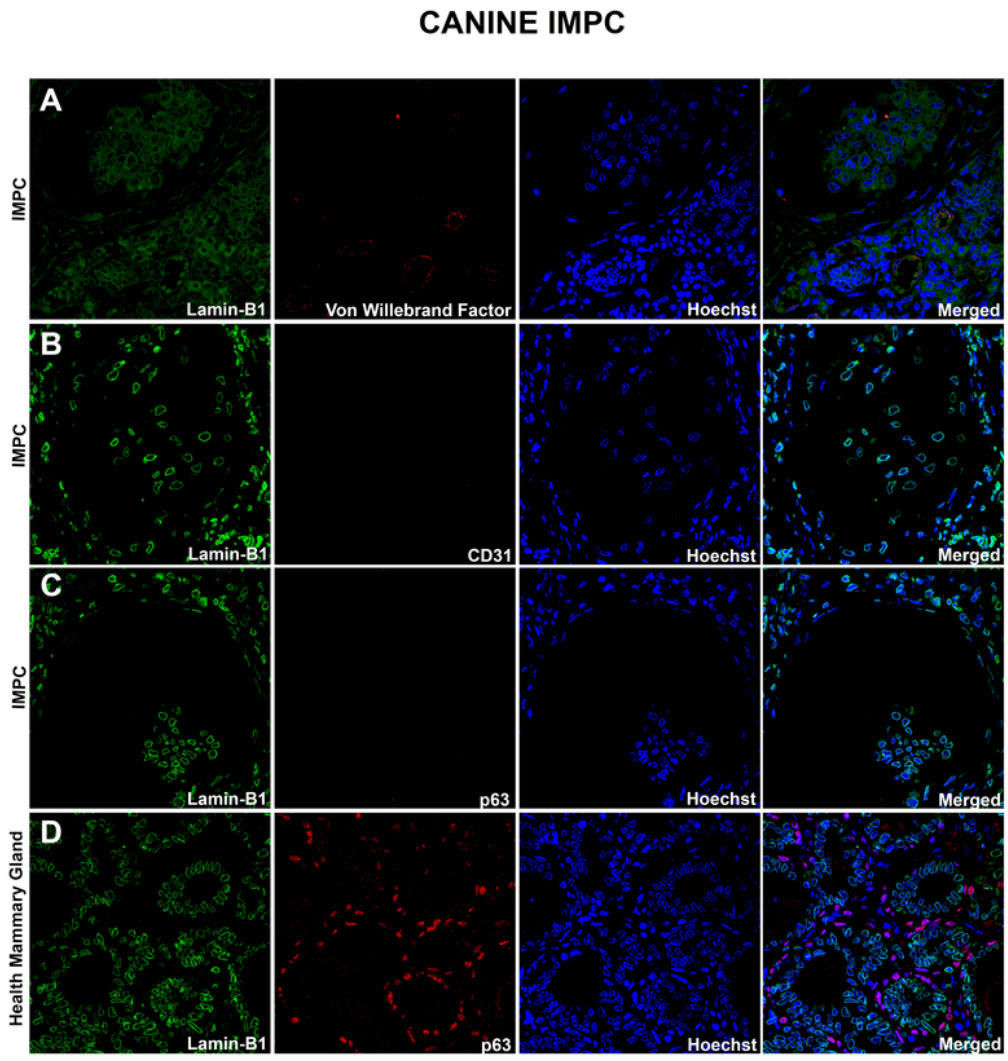

Figure 4

Figure 4

Absence of Von Willebrand Factor, CD31, and p63 labeling in the cystic spaces of invasive micropapillary areas of the mammary gland. Super-resolution images of the nuclear envelope marker Lamin B1/B2 (green), Von Willebrand Factor (A), CD31 (B), and p63 (C) (red) and the nucleus was stained with Hoechst (blue). Note that the staining was negative for endothelial and lymphatic cell markers (CD31 or Von Willebrand Factor) in micropapillary areas. Myoepithelial cell marker p63 staining was negative in IMPC and positive in the control health mammary gland (D). The merged images show the channels overlap. Images are representative of what was observed in n=40 separate primary tumor cases and were collected ten images from in situ and invasive areas of each case. Scale bars = 20 □m.

Figure 5

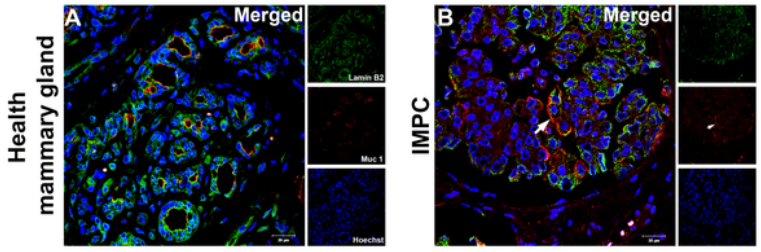

Figure 5

MUC1 expression in invasive micropapillary carcinoma of the canine mammary gland. Super-resolution merged images show the channels overlap of the nuclear envelope marker Lamin B1/B2 (green), MUC1 (red), and the nucleus was stained with Hoechst (blue). (A) MUC1 positive control showing apical staining in the health mammary gland. (B) Positive staining on the stroma-facing surface of the canine IMPC

cases (see white arrows). Images are representative of what was observed in 4 IMPC cases from the canine mammary gland and were collected ten images from invasive areas. Scale bars = 20 □m.

Figure 6

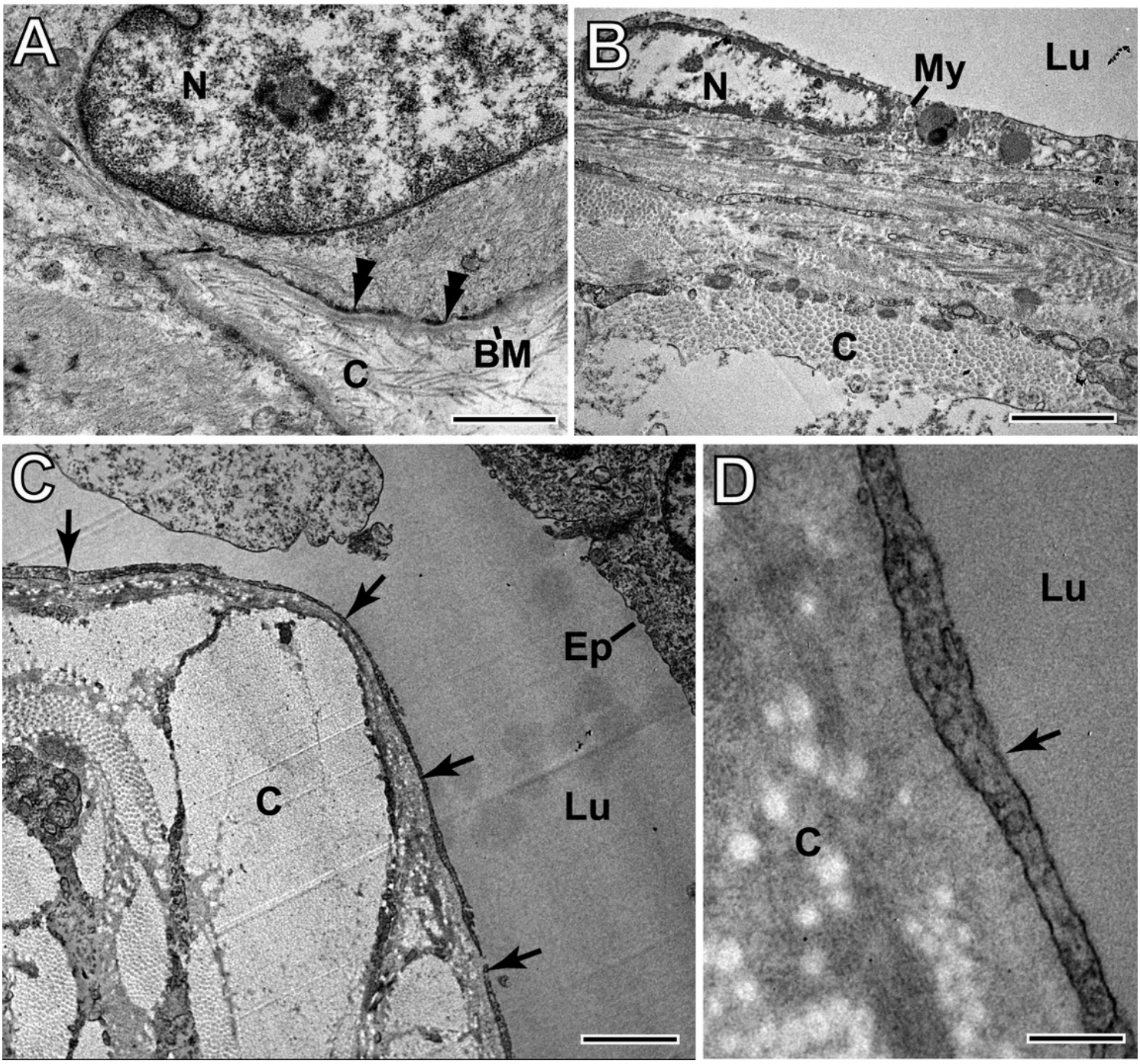

Figure 6

Ultrastructure of health and canine IMPC myoepithelial cell. (A) Healthy myoepithelial cell showing ovoid nuclear (N) shape and hemidesmosomes (double arrowheads) along the evident basement membrane (BM). In IMPC (B), myoepithelial cell (My) showing smaller and flatter nucleus and thinner cytoplasm. In

(C) and (D), observe thin cytoplasmic projections of My cells (arrows) coating the large lumen (Lu) of the cystic space, close to dense and ordered bundles of collagen fibrils (C). Ep, neoplastic epithelial cell. Scale bars: A-B, 1 µm; C, 2 µm; D, 200 nm.